CORE
Metadata, citation and similar papers at core.ac.uk
Provided by Cork Open Research Archive

Title	Transfer printing of AlGaInAs/InP etched facet lasers to Si substrates
Author(s)	Loi, Ruggero; O'Callaghan, James; Roycroft, Brendan; Robert, Cedric; Fecioru, Alin; Trindade, Antonio Jose; Gocalinska, Agnieszka; Bower, Christopher A.; Corbett, Brian
Publication date	2016-11-11
Original citation	Loi, R., Callaghan, J. O., Roycroft, B., Robert, C., Fecioru, A., Trindade, A. J., Gocalinska, A., Pelucchi, E., Bower, C. A. and Corbett, B. (2016) ' Transfer printing of AlGaInAs/InP etched facet lasers to Si substrates', IEEE Photonics Journal, 8(6), pp. 1-10. doi:10.1109/JPHOT.2016.2627883
Type of publication	Article (peer-reviewed)
Link to publisher's version	http://dx.doi.org/10.1109/JPHOT.2016.2627883 Access to the full text of the published version may require a subscription.
Rights	**© 2016 IEEE. Translations and content mining are permitted for academic research only. Personal use is also permitted, but republication/redistribution requires IEEE permission. See http://www.ieee.org/publications_standards/publications/rights/index.html for more information.**
Item downloaded from	http://hdl.handle.net/10468/3477

Downloaded on 2017-02-12T05:20:49Z

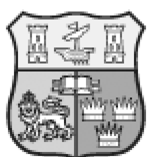

UCC
University College Cork, Ireland
Coláiste na hOllscoile Corcaigh

IEEE Photonics Journal
An IEEE Photonics Society Publication

Open Access

Transfer Printing of AlGaInAs/InP Etched Facet Lasers to Si Substrates

Volume 8, Number 6, December 2016

Ruggero Loi
James O'Callaghan
Brendan Roycroft
Cedric Robert
Alin Fecioru
Antonio Jose Trindade
Agnieszka Gocalinska
Emanuele Pelucchi
Chris Anthony Bower
Brian Corbett

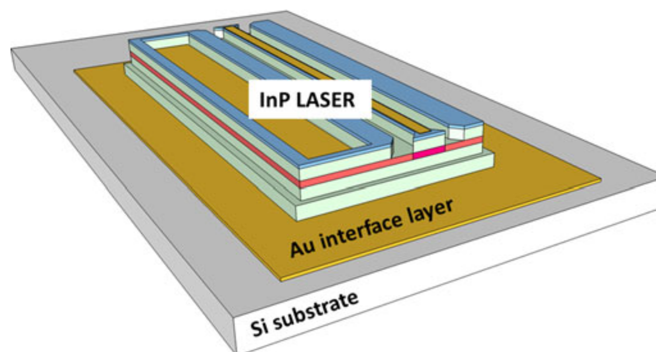

DOI: 10.1109/JPHOT.2016.2627883
1943-0655 © 2016 IEEE

IEEE photonics SOCIETY
IEEE

Transfer Printing of AlGaInAs/InP Etched Facet Lasers to Si Substrates

Ruggero Loi,[1] James O'Callaghan,[1] Brendan Roycroft,[1] Cedric Robert,[1] Alin Fecioru,[2] Antonio Jose Trindade,[2] Agnieszka Gocalinska,[1] Emanuele Pelucchi,[1] Chris Anthony Bower,[2] and Brian Corbett[1]

[1]Tyndall National Institute, University College Cork, Cork, Ireland
[2]X-Celeprint Ltd., Cork, Ireland

DOI:10.1109/JPHOT.2016.2627883
1943-0655 © 2016 IEEE. Translations and content mining are permitted for academic research only. Personal use is also permitted, but republication/redistribution requires IEEE permission. See http://www.ieee.org/publications_standards/publications/rights/index.html for more information.

Manuscript received September 22, 2016; revised November 7, 2016; accepted November 8, 2016. Date of publication November 11, 2016; date of current version November 29, 2016. This work was supported by Science Foundation Ireland under Irish Photonic Integration Centre Award 12/RC/2276 and enabled by the Irish Higher Education Authority Program for Research in Third Level Institutions (2007–2011) via the INSPIRE program. Corresponding author: R Loi (e-mail: ruggero.loi@tyndall.ie).

Abstract: InP-etched facet ridge lasers emitting in the optical C-band are heterogeneously integrated on Si substrates by microtransfer printing for the first time. 500 μm × 60 μm laser coupons are fabricated with a highly dense pitch on the native InP substrate. The laser epitaxial structure contains a 1-μm-thick InGaAs sacrificial layer. A resist anchoring system is used to restrain the devices while they are released by selectively etching the InGaAs layer with $FeCl_3$:H_2O (1:2) at 8 °C. Efficient thermal sinking is achieved by evaporating Ti–Au on the Si target substrate and annealing the printed devices at 300 °C. This integration strategy is particularly relevant for lasers being butt coupled to polymer or silicon-on-insulator (SOI) waveguides.

Index Terms: Heterogeneous integration, optical devices, infrared lasers, photonic materials and engineered photonic structures, fabrication and characterization.

1. Introduction

Driven by increasing global IP traffic, there are growing opportunities for III-V based semiconductor photonics components to be used in a diverse range of applications. These components need to be provided at low cost and should ideally scale in similar manner to silicon electronics. Nevertheless, due to the specific nature of individual III-V photonic components (lasers, modulators, detectors), it is highly challenging to monolithically integrate all these functions on a single substrate without compromising the performance of the individual devices [1], [2]. Thus, in general, a heterogeneous integration approach can be an effective way to combine optimized components for different photonic integrated circuits (PICs) [3]. This would lead to the photonics components not being stand-alone but being co-integrated with different electronic and wave-guiding platforms. Silicon photonics, which is addressing many different opportunities and particularly optical interconnections for data centers, is an excellent platform for scaling photonics due to its similarity with the principles of the semiconductor electronics industry [4]–[7]. High-quality functional PICs have been realized with very high structural precision (nm scale) using large diameter (300 mm) silicon-on-insulator (SOI) wafers [8]. Due to the lack of optical gain in silicon, an amplifier component needs to be integrated with the

SOI waveguide in order to provide a gain medium and enable the most functional PICs. The light from an external laser source can be coupled to a PIC using a grating coupler [9] or by butt coupling to a mode transformer [10] [11] [12]. In order to reduce the architectural complexity of PICs, III-V active components are usually integrated by flip chip wafer bonding or die-to-wafer bonding [13]. The coupons of III-V gain material are bonded directly, by molecular bonding, using a low temperature O_2 plasma-assisted surface activation or with an adhesive layer, usually Benzocyclobutene (BCB). The light can then be coupled to the waveguide by butt coupling [14], [15], grating coupling [16] or by evanescent coupling [17] through the use of tapers. Together with gratings on the Si this allows the realization of DBR and DFB lasers [18] [19] [20]. An alternative approach which potentially makes the heterogeneous integration faster and more scalable is the micro transfer print (μTP) technique [21]. In μTP arrays of components are released from their native growth substrate and transferred with $\pm$ 1 μm positional accuracy to a locally flat non-native target substrate. The components can then be electrically and optically integrated with other functions on the new substrate. μTP has been used to release a wide range of LEDs, lasers, detectors and photovoltaic cells onto rigid and flexible target substrates [22], [23], directly or with adhesive layers [24]. GaAs-based lasers have been heterogeneously integrated by μTP with pre- or post-fabrication [25], [26]. However, for applications in the telecommunication wavelength range it is necessary to work with InP-based materials as these provide the most mature laser structures. The heterogeneous integration of an InP-based coupon to an SOI by μTP has been recently reported [27] where the light is evanescently coupled to a Si waveguide by tapers while an external light source pumps the active material to function as an LED. Another crucial issue in the heterogeneous integration of InP active elements to SOI platforms is the thermal sinking of the heat produced by the device in operation. In fact different strategies based on thermally conductive vias have been explored [13], [28], [29] to overcome high thermal impedances which could arise at the bonding interface or by the introduction of thermally insulating bonding layers.

In this paper, we introduce a new strategy for heterogeneous integration of InP etched facet lasers to Si substrates by using μTP. The use of an etched facet technology allows the prefabrication of the devices in standard foundry facilities and allows the cavity to be aligned independently of the crystal orientation. Efficient light coupling to a polymer waveguide can be attained by butt coupling [15]. The wafer structure incorporates an InGaAs release layer which allows the separation of the devices from their native InP substrate and their subsequent transfer printing to a silicon substrate [30]. The printed devices show continuous wave lasing in the C-band, and improved thermal sinking is achieved by introducing a metal bonding layer and a controlled annealing step in the print process.

2. Experimental Method

Dense arrays of Fabry-Perot lasers with up to 2000 devices per cm^2 on a fixed pitch are fabricated on the native InP substrate using lithography and anisotropic Inductively Coupled Plasma (ICP) etching techniques to form the laser mirrors together with a conventional ridge waveguide. The lasers are fabricated as rectangular coupons and are held in place by a resist anchoring system which allows them to be undercut by wet etching. Finally, the device coupons are transferred to the non-native substrate by means of μTP. The overall process flow is shown schematically in Fig. 1.

2.1. Laser Wafer

The epitaxial structure is grown by metal organic vapour phase epitaxy with nitrogen as the carrier gas [31], [32]. Six 6-nm-thick compressively-strained AlInGaAs quantum wells and seven 10 nm thick tensile strained barriers form the 96 nm thick MQW active region in a step index waveguide of 326 nm total thickness. The waveguide is clad by 1.5-μm-thick n- and p- doped InP. A p-doped InGaAs contact layer is finally grown. In addition, a 1-μm-thick InGaAs n-doped (1×10^{18} cm^{-3}) sacrificial layer has been included between the substrate and the n-InP cladding layer of the laser to allow the release of the devices from the native wafer by means of a selective wet etch. The n-type doping makes the InGaAs layer electrically conductive in order to evaluate the lasers on the native

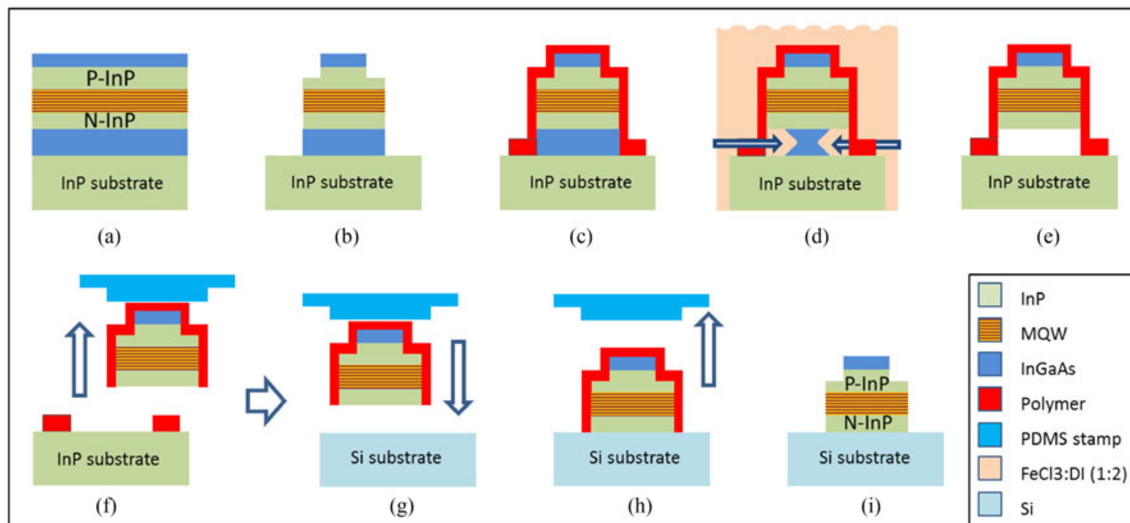

Fig. 1. Devices are fabricated on an InP wafer including an InGaAs release layer at the bottom of the epitaxial structure (a), (b). An anchor system made of polymer (resist) keeps the devices in place (c) during the undercut while allowing the etchant to penetrate underneath the mesas through some openings (d), (e). Finally, the devices are picked up (f) and transfer-printed onto the new substrate using a Polydimethylsiloxane (PDMS) stamp (g)–(i).

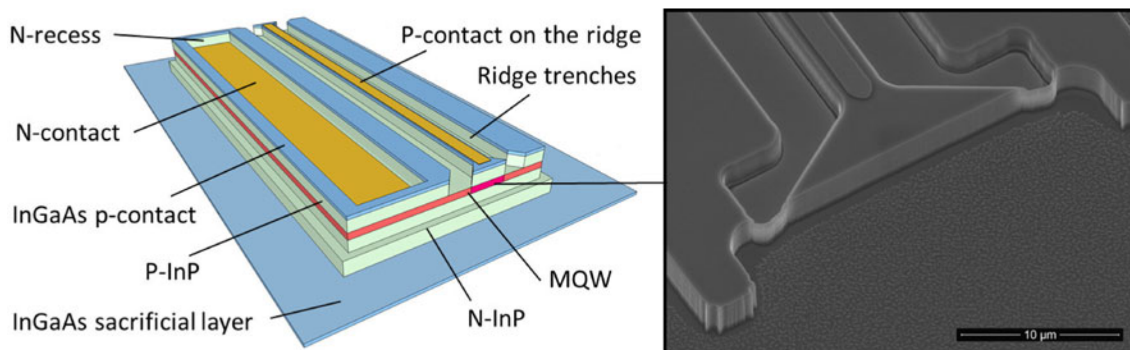

Fig. 2. Diagram of a laser geometry used and epitaxial structure arrangement before etching through the sacrificial layer; p- and the n-contact are on the epitaxial side of the device. The right-hand side shows the Scanning Electron Microscope (SEM) image of the etched facet prior to its passivation with SiN.

substrate with a contact on the substrate side before the transfer printing. The transverse mode of the epitaxial structure has a size of 1 μm with a mode overlap of 6.6% with the quantum wells. The transverse mode reaches 0.5 μm into the InP cladding layers making the mode independent of the contact layer or features on the substrate side. This strategy makes this epitaxial structure particularly adapt for transferable devices.

2.2. Laser Design And Fabrication

A nine-level lithography process has been developed to realize lasers suitable for transfer printing. The laser devices are fabricated before the transfer providing arrays of ridge-waveguide lasers in rectangular coupons with both anode and cathode on the epitaxial side (see Fig. 2). ICP etching of the facets allows the cavity to be independent of the crystal direction as it does not require cleaving. Initially a 10 nm /110 nm Ti/Au p-type contact metal is deposited. Next, a 2.5-μm waveguide ridge

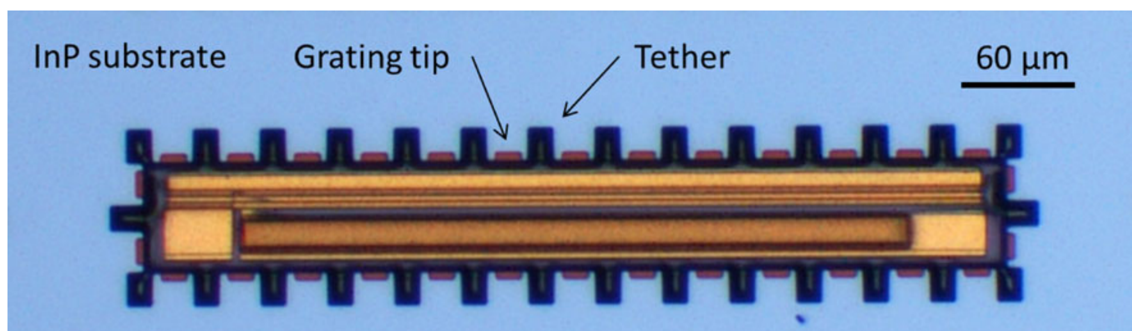

Fig. 3. Top view of a laser coupon ready for undercut with the polymer anchor system in place. The starting points for the etchant are visible between the tethers (grating tip).

is defined. The ridge depth is about 1.5 μm and stops before the Multi Quantum Well (MQW) active region in order to control the optical confinement and losses while minimizing the current leakage. The ridge extends to the edge of the facets with a V shape so as to prevent the ridge etch from affecting the quality of the etched facet. The reduction in effective facet reflectivity due to diffraction in the taper region is numerically calculated to be 0.9%. An ICP dry etch using Cl_2 / H_2 / CH_4 chemistry defines the facets for the Fabry-Perot laser cavity together with the rectangular device coupons and an opening for the n-contact (see Fig. 2). The resonator length is 500 μm on every coupon. A flat evaporation of a 14 nm /14 nm /14 nm /11 nm /200 nm of Au /Ge /Au /Ni /Au defines the n-contact on the devices. The sidewalls and the facets are encapsulated with a SiN layer in order to protect the facets during the undercut and following steps of fabrication.

A low-temperature anneal at 300 °C for 30 minutes was required to form a low resistance ohmic contact to the n-type InP layer. A final metal evaporation provides contact pads for electrical characterization. The resulting coupons have designs with different areas and pads geometries (see Fig. 3 and 4), with coupon lengths in the range of 500-600 μm and widths of 40 μm and 60 μm. A final ICP dry etch through the InGaAs sacrificial release layer reaches the InP substrate. A coarse grating shaping on the release layer around the coupons provides an initial starting location to the etchant which helps to manage the initial etch front (see Fig. 3). Finally a 2.8 μm thick resist layer is patterned with tethers to anchor the mesas to the substrate during the undercut step. The resist anchors give an additional protective layer to the coupon encapsulation and need to withstand the etchant for the duration of the undercut. The evaluation of the capillary forces acting underneath the devices is fundamental to avoid the coupons detaching during the undercut, rinse or drying steps. The opening between one tether and the next allows the etchant to penetrate underneath the coupons. Another important feature for the anchor system is the easy breakage of the tethers to facilitate the pick-up of the devices during transfer printing while not creating debris or flaps. Different anchor systems with various tethers shapes and dimension were tested (see Fig. 4). The tests demonstrated the best configuration with a tethers spacing of 40 μm and 15 μm wide tethers having a tapered narrowing to 5 μm at 10 μm distance to the coupon and by using the largest foot anchoring area. These parameters provide the best adhesion to the InP substrate and a good stability during the undercut while allowing easy and clean breaking of the tethers during the pick-up step.

2.3. *Undercut*

Wet etching of the sacrificial layer has been investigated in order to obtain released devices with flat and smooth bottom surfaces to ensure the best adhesion of the devices on the new substrate. The etch rates along different crystal directions of the release layer and the selectivity over InP were investigated for three different etching solutions: phosphoric-peroxide, citric-peroxide and iron chloride (see Table 1). The experiments have been conducted on a wafer processed to create a pattern of rectangular coupons (mesas) of 500 μm in length and with different widths (from 40 μm

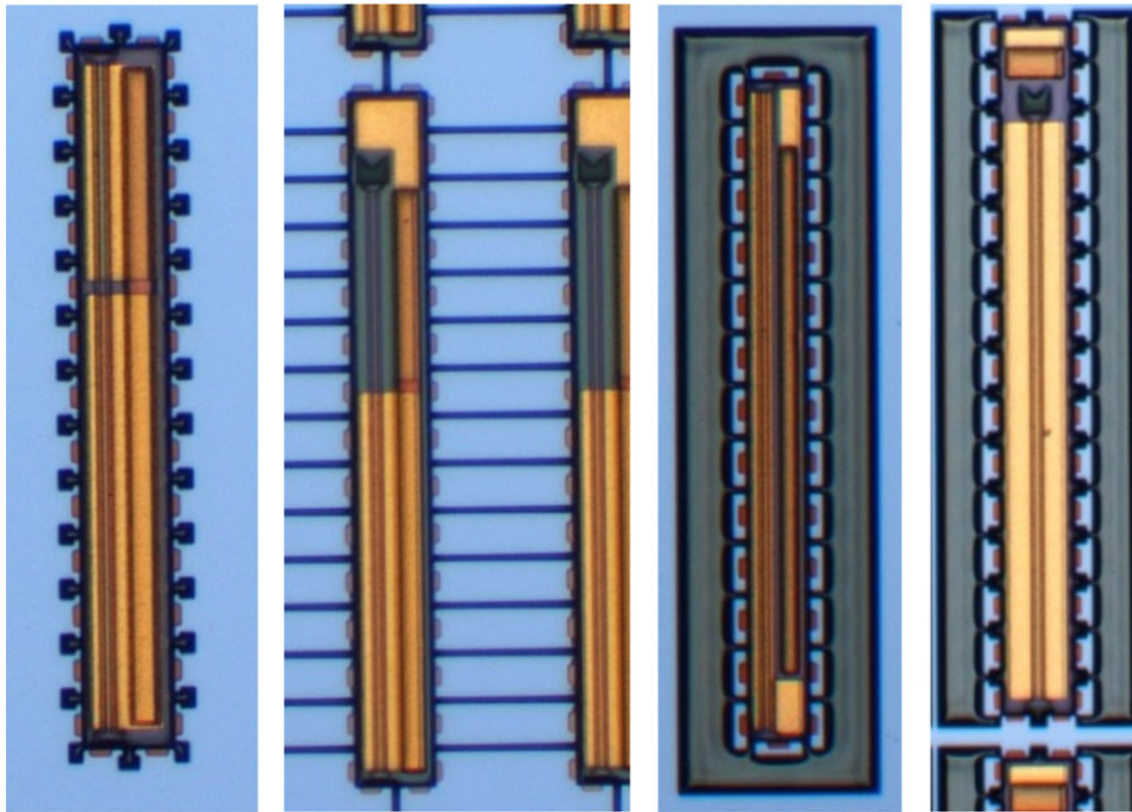

Fig. 4. Optical microscope images of 60 μm and 40 μm wide laser coupons having different metal probe pads arrangements and anchor geometries. The pad arrangement which is easier to be fabricated and electrically probed is on the left. The most reliable anchor system found is the last on the right, and it results in less debris formation during the pick-up and gives the highest yield of restrained device after the undercut thanks to its shrank connection to the coupon and a large foot anchoring area.

TABLE 1

InGaAs and InP Etch Characteristics for Different Etchant Solutions at 18 °C

Etchant	Composition	Lateral Etch rate <010> (InGaAs) nm/min	Vertical Etch rate <100> (InGaAs) nm/min	Vertical Etch rate <100> (InP) nm/min	Selectivity (InGaAs/InP)
Phosphoric-Peroxide	H_3PO_4:H_2O_2: H_2O (1:1:8)	315	250	0.4	787
Citric-Peroxide	$C_6H_8O_7$: H_2O_2 (7:1)	175	30	0.3	585
Iron Chloride	$FeCl_3$: H_2O (1:2)	1330	530	1.8	735

to 120 μm) arranged at 45° angle [see Fig. 5(a)] with respect to the major axes of the crystal. Such a layout allows the exploitation of the anisotropic behavior of the etchants [33] while giving an etch front that retains the rectangular coupon profile. The even evolution of the etch front reduces uneven stresses on the coupon due to capillary forces during the undercut and prevents formation of defects on the bottom surface of the coupons. The tests showed the highest lateral etch rate of InGaAs is obtained with the $FeCl_3$ based solution along the <010> and <001> crystal planes and

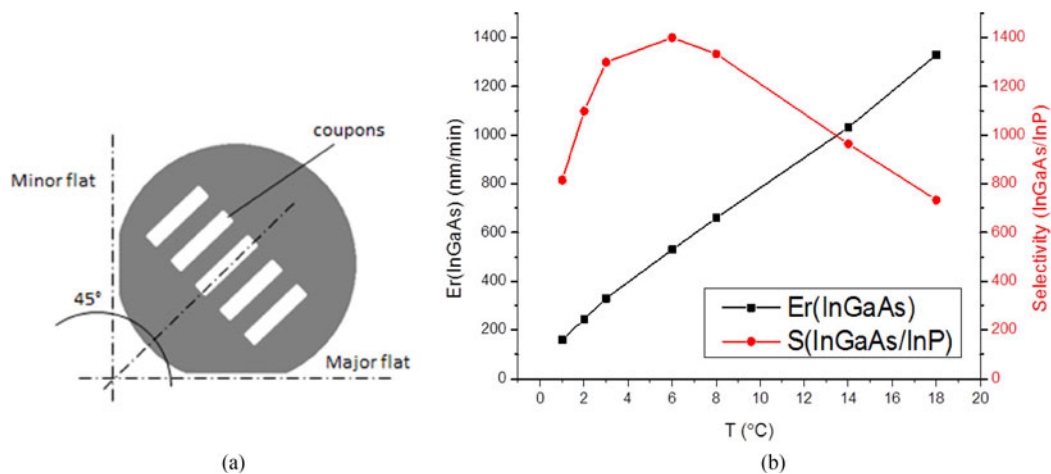

Fig. 5. Coupon arrangement with respect to the crystal planes of the wafer (a); the <010> and <001> crystal planes are at 45° to the major axis. Etch-rate of $FeCl_3$:H_2O (1:2) for InGaAs along <010> and <001> planes and the related selectivity to InP for bath temperatures in the range 1-18 °C (b).

is 1330 nm/min at 18 °C. The selectivity, S, has been calculated as the ratio between the lateral etch rate of InGaAs and the vertical etch rate of InP along the <100> crystal planes. The best selectivity at 18 °C is given by the phosphoric based solution and the $FeCl_3$:H_2O respectively at $S = 787$ and $S = 735$. Sacrificial mesas which were 5 μm longer and wider than the other coupons and without anchor system were used to monitor the etch progress during the undercut.

The etch rate and selectivity were studied for temperatures in the range of 1-18 °C [see Fig. 5(b)] as the $FeCl_3$:H_2O selectivity has been reported to increase at lower temperatures [33]. A cold-tunable plate was used to keep the temperature constant during the etching with an accuracy of ±0.1 °C. When the bath temperature is decreased from 18 °C to 1 °C the etch rate of iron chloride decreases almost linearly to 160 nm/min along the <010> and <001> planes. Nevertheless, there is an increase in the selectivity to InP by a factor 2 at temperatures between 2 °C and 12 °C which results in released surfaces with improved flatness and superficial roughness while also allowing the release of wider coupons. As a result the profile of a 60 μm wide coupon at the bottom has a deviation from flatness of less than 20 nm and a surface roughness $S_q = 2.2$ nm. This allows the undercut of a 60 μm wide coupon in approximately 50 minutes at 8 °C. At temperatures lower than 1 °C the transport of the etchant beneath the mesas reduces and some solid residuals are generated due to $FeCl_3$ precipitation or ice formation affecting the etch homogeneity and the cleanliness of the sample. The precipitation phenomenon is linked to the lower solubility threshold of $FeCl_3$ in deionized water as the temperature decreases. The erosion of the resist tethers is negligible in the temperature range studied.

2.4. Micro Transfer Printing

A transparent PDMS elastomeric stamp is used in μTP technology to retrieve and deterministically assemble arrays of devices onto non-native substrates. This technology collects or releases the devices by simply varying the speed of the PDMS stamp according with peel-rate-dependent adhesion in viscoelastic elastomers [21], [22], [34], [35]. The 3.5-μm-thick laser coupons were transferred onto the target substrate at temperatures in the range of $18 - 110$ °C. The highest yield of correctly printed devices is obtained at the highest temperature. Printing temperatures higher than 110 °C cause the resist to reflow which could affect the printing. The laser devices were printed on glass, silicon and gold coated silicon substrates [see Fig. 6(a) and (b)]. The printing on glass allowed monitoring of the flatness of the bottom surface of the coupons and the bonding to the substrate in order to optimize the process parameters. When the surfaces are sufficiently flat, no

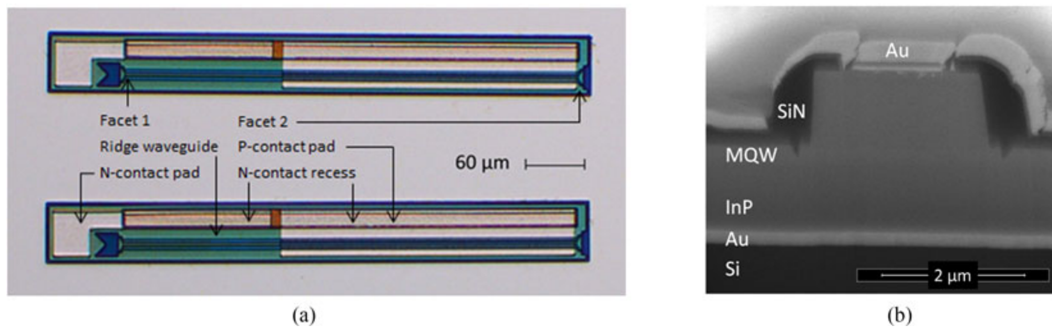

Fig. 6. Top view of two laser coupons printed on an Au coated Si substrate (a). The various device elements are illustrated. A Focused Ion Beam (FIB) cross section of the ridge region (b) shows defect free bonding between the laser and the Au coated Si substrate.

shadowed areas or interference fringes are visible through the glass. In this case the coupons are bonded to the substrate by van der Waals forces which are strong enough to permit subsequent processing steps and electrical probing without having the coupons moving from the original site. For the adhesiveless printing employed here a deviation of flatness of more than 30 nm results in a lower yield of printed devices by reducing the contact area between the device and the substrate. This would lead to a decrease in the thermal sinking and in the adhesion. The best device performances were obtained by a further improvement in heat sinking achieved by depositing a Ti/Au (10 nm/100 nm) layer onto the Si substrate prior to the transfer. After the printing step the resist is removed by oxygen plasma and solvents.

3. Results

Electro-optical tests of the devices before and after the transfer print determined the laser performance and the variation introduced by the transfer onto different substrates. The voltage current (V I) and the light current (LI) measurements were performed both in pulsed and continuous wave modes. The light power was detected by placing a 3 mm diameter Ge detector a few mm from the facets of the printed lasers and maximizing the light collection by adjusting the detector position with a movable stage. In this configuration it is possible to collect a portion of emitted light which approximates the LI characteristic of the device.

The lasers before transfer have a threshold current, I_{th}, of 45 mA and resulting threshold current density J_{th} at 600 A/cm^2 per quantum well, at room temperature (18 °C). J_{th} is about three times higher than that of similar cleaved facet devices. This can be ascribed to a low reflection at the facets due to SiN coating being thinner than λ/n which reduces the mirror reflectivity. It should also be noted that there is an important role played by the release layer in heat sinking as InGaAs has a thermal conductivity $\sigma(\text{InGaAs}) = 0.05\,\text{W}\,\text{cm}^{-1}{}^{\circ}\text{C}^{-1}$, which is about one order of magnitude lower than $\sigma(\text{InP}) = 0.68\,\text{W}\,\text{cm}^{-1}{}^{\circ}\text{C}^{-1}$ and thus the InGaAs acts as a thermal insulator layer increasing the thermal impedance of the devices on the native substrate. The increased heating and low reflectivity results in the devices operating only in pulsed mode (duty cycle $D = 0.1\%$, $T = 500\,\mu\text{s}$) before transfer.

The lasers printed on plain Si have I_{th} of 45 mA at 18 °C, in pulsed mode. In this case it is possible to use duty cycles up to two orders of magnitude higher than the case for devices on the native substrate. The improved performance is most likely due to the increased thermal sinking associated with the removal of the InGaAs layer. The thermal conductivity of silicon $\sigma(\text{Si}) = 1.3\ \text{Wcm}^{-1}{}^{\circ}\text{C}^{-1}$ is about twenty six times higher than $\sigma(\text{InGaAs})$. Moreover, finite element simulations reveal that is possible to take advantage of the increased thermal conductivity of the new substrate when the distance between the heat-generating layer and the substrate is less than 3 μm [36]. Here the separation between the MQW region and the Si substrate was 1.5 μm.

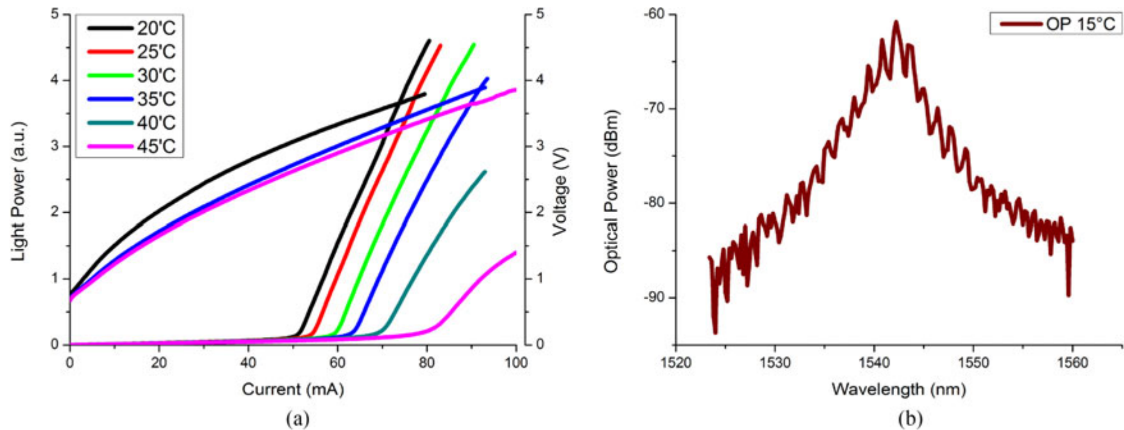

Fig. 7. LI and VI curves for temperatures in the range 20–45 °C (a) and spectrum (b), for a laser with the facets passivated by SiN and printed on Au coated Si.

The printing of the lasers on the Au coated Si introduced a net improvement in the thermal sinking allowing lasing in continuous wave mode (Fig. 7). The improved thermal sinking with the Au layer having a higher thermal conductivity than Si, $\sigma(\mathrm{Au}) = 3.14\,\mathrm{W\,cm^{-1}\,{}^{\circ}C^{-1}}$. The quality of the bond can be improved by thermal annealing at 300 °C. I_{th} was around 45 mA at room temperature and varies from 50 mA to 80 mA for a change in the stage temperature from 20 °C to 45 °C. The value of the characteristic temperature, T_0, of the threshold current is calculated to 57.5 K.

The emission spectrum was collected by using a multimode fiber positioned at few millimeters in front of the lasers which were printed on Au coated Si. Fig. 7(b) shows the main emission peak at 1542 nm at room temperature. The free spectral range of the resonator $\Delta\lambda$ is given by $\lambda_0^2/2nL$, where n is the group index in the resonator, L is the cavity length, and λ_0 is the light wavelength. The expected $\Delta\lambda$ for L $\sim$500 μm is in agreement with the measured value $\Delta\lambda_{\mathrm{exp}} = 0.66\,\mathrm{nm}$.

4. Conclusion

We have demonstrated the key processing steps for the release of InP-based etched facet ridge lasers from the donor InP substrate and the μTP to Si substrates with and without metal bonding layers. Lasers printed on Au coated silicon are shown to operate in a continuous-wave manner up to 45 °C. The performance can be improved by engineering the reflectivity at the facets. The electro-optical characterization shows that a significant challenge is in managing the heat dissipation from the printed lasers to the substrate. The annealing of the coupon at 300 °C improves the adhesion to the target substrate while providing an excellent thermal sink and consequently low thermal impedance to the devices. This reduces the complexity of the integration given by the use of adhesive layers as, for example, BCB, which requires the engineering of thermal vias to overcome its low thermal conductivity of 0.0029 $\mathrm{Wcm^{-1}\,{}^{\circ}C^{-1}}$ at 25 °C. The optical mode of the epitaxial structure has minimal interaction with the new substrate facilitating the use of the etch facet technology while making the devices suitable for transfer printing. The etched facet configuration permits new geometries which can be suitable for easier heterogeneous integration of InP lasers on PICs. The laser light output can be subsequently coupled directly to polymeric waveguides using lithographic techniques or it can be down-coupled to Si waveguides by appropriate engineering of tapers. This work shows that μTP is a suitable technique for wafer-scale integration of high-performance InP lasers onto Si and other substrates. The stamps can be designed to transfer hundreds to thousands of discrete coupons in a single pickup and print operation. The μTP technique is not sensitive to the wafer-size mismatch problems or the need for large flat regions as required for wafer bonding. In addition, multiple prints can be employed to transfer many different device types leading to

versatile integration strategies. These features position μTP as one of the main techniques for heterogeneous integration of III-V to Si.

Acknowledgment

The authors would like to thank the staff of the clean-room at Tyndall National Institute for the assistance provided during the fabrication of the devices and the accomplishment of the undercut tests.

References

[1] H. Park *et al.*, “Device and integration technology for silicon photonic transmitters,” *IEEE J. Sel. Top. Quantum Electron.*, vol. 17, no. 3, pp. 671–688, May/Jun. 2011.
[2] P. Dong, Y. K. Chen, G. H. Duan, and D. T. Neilson, “Silicon photonic devices and integrated circuits,” *J. Nanophoton.*, vol. 3, pp. 215–228, 2014.
[3] G. H. Duan *et al.*, “New advances on heterogeneous integration of IIIV on silicon,” *IEEE J. Lightw. Technol.*, vol. 33, no. 5, pp. 976–983, Mar. 2015.
[4] R. Soref, “The past, present, and future of silicon photonics,” *IEEE J. Sel. Top. Quantum Electron.*, vol. 12, no. 6, pp. 1678–1687, Nov./Dec. 2006.
[5] M. Hochberg and T. Baehr-Jones, “Towards fabless silicon photonics,” *Nature Photon.*, vol. 4, no. 8, pp. 492–494, 2010.
[6] S. Assefa, F. Xia, W. M. J. Green, C. L. Schow, A. V. Rylyakov, and Y. A. Vlasov, “CMOS-integrated optical receivers for on-chip interconnects,” *IEEE J. Sel. Topics Quantum Electron.*, vol. 16, no. 5, pp. 1376–1385, Sept./Oct. 2010.
[7] G. Li *et al.*, “Ultralow-loss, high-density SOI optical waveguide routing for macrochip interconnects,” *Opt. Exp.*, vol. 20, no. 11, pp. 12035–12039, 2012.
[8] S. Selvaraja *et al.*, “Highly uniform and low-loss passive silicon photonics devices using a 300 mm CMOS platform,” in *Proc. Opt. Fiber Commun. Conf. Exhib.*, 2014, Paper Th2A.33.
[9] A. Huang *et al.*, “A 10 Gb/s photonic modulator and WDM MUX/DEMUX integrated with electronics in 0.13 m SOI CMOS,” in *Proc. IEEE Int. Solid State Circuits Conf.*, 2006, vol. 922, pp. 922–929.
[10] N. Hatori *et al.*, “A hybrid integrated light source on a silicon platform using a trident spot-size converter,” *J. Lightw. Technol.*, vol. 32, no. 7, pp. 1329–1336, Apr. 2014.
[11] J. H. Lee *et al.*, “Demonstration of 12.2% wall plug efficiency in uncooled single mode external-cavity tunable Si/III-V hybrid laser,” *Opt. Exp.*, vol. 23, no. 9, pp. 12079–12088, 2015.
[12] M. Lamponi *et al.*, “Low-threshold heterogeneously integrated InP/SOI laser with a double adiabatic taper coupler,” *IEEE Photon. Technol. Lett.*, vol. 24, no. 1, pp. 76–78, Jan. 2012.
[13] G. Roelkens *et al.*, “III-V/silicon photonics for on-chip and intra-chip optical interconnects,” *Laser Photon. Rev.*, vol. 4, pp. 1–29, 2010.
[14] G. Roelkens, D. Van Thourhout, R. Baets, R. Ntzel, and M. Smit, “Laser emission and photodetection in an InP/InGaAsP layer integrated on and coupled to a silicon-on-insulator waveguide circuit,” *Opt. Exp.*, vol. 14, pp. 8154–8159, 2006.
[15] R. Tseng *et al.*, “Laser integration with CMOS assembly process for Si photonics,” in *Proc. Opt. Fiber Commun. Conf. Exhib.*, 2014, Paper Th2A.41.
[16] B. Song, C. Stagarescu, S. Ristic, A. Behfar, and J. Klamkin, “3D integrated hybrid silicon laser,” *Opt. Exp.*, vol. 24, no. 10, pp. 10435–10444, 2016.
[17] A. W. Fang, H. Park, O. Cohen, R. Jones, M. J. Paniccia, and J. E. Bowers, “Electrically pumped hybrid AlGaInAs-silicon evanescent laser,” *Opt. Exp.*, vol. 14, no. 20, pp. 9203–9210, 2006.
[18] A. W. Fang *et al.*, “A distributed bragg reflector silicon evanescent laser,” *IEEE Photon. Technol. Lett.*, vol. 20, no. 20, pp. 1667–1669, Oct. 2008.
[19] A. W. Fang, E. Lively, Y. H. Kuo, D. Liang, and J. E. Bowers, “A distributed feedback silicon evanescent laser,” *Opt. Exp.*, vol. 16, pp. 4413–4419, 2008.
[20] B. B. Bakir *et al.*, “Electrically driven hybrid Si/III-V lasers based on adiabatic mode transformers,” *Opt. Exp.*, vol. 19, no. 11, pp. 10317–10325, 2011.
[21] M. A. Meitl *et al.*, “Transfer printing by kinetic control of adhesion to an elastomeric stamp,” *Nature Mater.*, vol. 5, pp. 33–38, 2006.
[22] J. Yoon, S. M. Lee, D. Kang, M. A. Meitl, C. A. Bower, and J. Rogers, “Heterogeneously integrated optoelectronic devices enabled by microtransfer printing,” *Adv. Opt. Mater.*, vol. 3, no. 10, pp. 1313–1335, 2015.
[23] H. Yang *et al.*, “Transfer printing stacked nanomembrane lasers on silicon,” *Nature Photon.*, vol. 6, pp. 617–622, 2012.
[24] A. Carlson, A. M. Bowen, Y. Huang, R. G. Nuzzo, and J. A. Rogers, “Transfer printing techniques for materials assembly and micro/nanodevice fabrication,” *Adv. Mater.*, vol. 24, pp. 5284–5318, 2012.
[25] J. Justice, C. A. Bower, M. Meitl, M. B. Mooney, M. A. Gubbins, and B. Corbett, “Wafer-scale integration of group III-V lasers on silicon using transfer printing of epitaxial layers,” *Nature Photon.*, vol. 6, no. 9, pp. 610–614, 2012.
[26] X. Sheng, C. Robert, S. Wang, G. Pakeltis, B. Corbett, and J. A. Rogers, “Transfer printing of fully formed thinfilm microscale GaAs lasers on silicon with a thermally conductive interface material,” *Laser Photon. Rev.*, vol. 9, no. 4, pp. L17–L22, 2015.
[27] A. De Groote *et al.*, “Transfer-printing based integration of single-mode waveguide-coupled III-V-on-silicon broadband light emitters,” *Opt. Exp.*, vol. 24, pp. 13754–13762, 2016.
[28] G. Roelkens *et al.*, “III-V/Si photonics by die-to-wafer bonding,” *Mater. Today*, vol. 10, no. 7/8, pp. 1369–7021, 2007.

[29] M. N. Sysak *et al.*, “Hybrid silicon laser technology: A thermal perspective,” *IEEE J. Sel. Topics Quantum Electron.*, vol. 17, no. 6, pp. 1490–1498, Nov./Dec. 2011.

[30] R. Loi *et al.*, “Technologies for transfer printing of InP based etched facet lasers,” in *Proc. MRS Spring Meeting Exhib.*, 2016, Paper EP7.4.03. [Online]. Available: http://www.mrs.org/spring-2016-program-ep7/

[31] V. Dimastrodonato, L. O. Mereni, R. J. Young, and E. Pelucchi, “AlGaAs/GaAs/AlGaAs quantum wells as a sensitive tool for the MOVPE reactor environment,” *J. Cryst. Growth*, vol. 312, pp. 3057–3062, 2010.

[32] A. Gocalinska, M. Manganaro, E. Pelucchi, and D. D. Vvedensky, “Surface organization of homoepitaxial InP films grown by metalorganic vapor-phase epitaxy,” *Phys. Rev. B*, vol. 86, 2012, Art. no. 165307.

[33] T. Kusserow *et al.*, “Micromachining of InP/InGaAs multiple membrane/airgap structures for tunable optical devices,” *Proc. SPIE*, vol. 6993, Apr. 2008, Art. no. 69930B.

[34] T. H. Kim *et al.*, “Kinetically controlled, adhesiveless transfer printing using microstructured stamps,” *Appl. Phys. Lett.*, vol. 94, 2009, Art. no. 113502.

[35] A. Carlson *et al.*, “Shear-enhanced adhesiveless transfer printing for use in deterministic materials assembly,” *Appl. Phys. Lett.*, vol. 98, 2011, Art. no. 264104.

[36] Z. H. Quan, J. Justice, M. B. Mooney, M. A. Gubbins, P. J. Parbrook, and B. Corbett, “Thermal modeling of transfer bonded thin-film gallium arsenide laser diode,” *IET Optoelectron.*, vol. 10, no. 2, pp. 51–56, 2016.